An Investigation of LSF-YSZ Conductive Scaffolds for Infiltrated SOFC Cathodes

Yuan Cheng,[a] Tae-Sik Oh,[a,b,*] Rachel Wilson,[a] Raymond J. Gorte,[a,*] and John M. Vohs[a,*,z]

[a]*Department of Chemical and Biomolecular Engineering, University of Pennsylvania, Philadelphia, Pennsylvania 19104, USA*
[b]*Department of Chemical Engineering, Auburn University, Auburn, Alabama 36849, USA*

Porous composites of Sr-doped $LaFeO_3$ (LSF) and yttria-stabilized zirconia (YSZ) were investigated as conductive scaffolds for infiltrated SOFC cathodes with the goal of producing scaffolds for which only a few perovskite infiltration steps are required to achieve sufficient conductivity. While no new phases form when LSF-YSZ composites are calcined to 1623 K, shifts in the lattice parameters indicate Zr can enter the perovskite phase. Measurements on dense, LSF-YSZ composites show that the level of Zr doping depends on the Sr:La ratio. Because conductivity of undoped LSF increases with Sr content while both the ionic and electronic conductivities of Zr-doped LSF decrease with the level of Zr in the perovskite phase, there is an optimum initial Sr content corresponding to $La_{0.9}Sr_{0.1}FeO_3$ (LSF91). Although scaffolds made with 100% LSF had a higher conductivity than scaffolds made with 50:50 LSF-YSZ mixtures, the 50:50 mixture provides the optimal interfacial structure with the electrolyte and sufficient conductivity, providing the best cathode performance upon infiltration of $La_{0.6}Sr_{0.4}Co_{0.2}Fe_{0.8}O_3$ (LSCF).
 [DOI: 10.1149/2.0531706jes]

Manuscript submitted January 31, 2017; revised manuscript received March 10, 2017. Published March 24, 2017.

The common method for fabricating state-of-the-art solid oxide fuel cells (SOFC) that use LSCF (Sr-doped $LaCo_{0.2}Fe_{0.8}O_3$) cathodes involves several high-temperature firing steps.[1] First, the NiO-YSZ composite that will become the anode is co-fired together with the YSZ electrolyte to produce a dense electrolyte. Next, a doped-ceria layer is screen printed onto the cathode side of the dense electrolyte and fired to produce a doped-ceria film that will act as a barrier layer to prevent reaction of the LSCF with the YSZ. Finally, LSCF is screen printed onto the doped-ceria film and fired to a temperature sufficient to give the LSCF structural integrity and good adhesion to the electrolyte. Obviously, there would be significant advantages to reducing the number of fabrication and calcination steps.

An alternative method for preparing high-performance LSCF cathodes involves preparing a porous YSZ scaffold on the cathode side of the electrolyte, followed by infiltration of LSCF nanoparticles or precursor salts.[2] The NiO-YSZ anode, the YSZ electrolyte, and the YSZ scaffold layers can all be co-fired, and the doped-ceria barrier layer may not be needed.[3] However, the infiltration method is not widely used because many infiltration steps are typically required to provide sufficient cathode conductivity.

Recently, it was suggested that the number of infiltration steps could be greatly reduced if the porous scaffold was itself electronically conductive.[4] Infiltration is still required to add LSCF into the scaffold to carry out the oxygen-exchange reactions but the amounts required for the catalytic reaction can be much smaller. To implement this approach, it is necessary to find a conductive oxide that will not react with YSZ at the temperatures required to produce a dense electrolyte. Because Sr-doped $LaFeO_3$ (LSF) has been shown to be relatively unreactive with YSZ,[5–7] our group focused on preparing LSF-YSZ scaffolds for this application.[4] Co-firing LSF and YSZ did not lead to new phases but a shift in the lattice parameter for the perovskite phase suggested that some Zr was entering the perovskite lattice. Electrochemical cells produced with the LSF-YSZ scaffolds exhibited reasonable performance; however, some ohmic losses were observed prior to infiltration of additional perovskite, suggesting that higher conductivities would be desirable. Zr doping of LSF is known to decrease its electronic conductivity[7] and this may be responsible for the low conductivity of the scaffold.

In the present study, we have further explored the use of LSF-YSZ composites as scaffolds for SOFC cathodes and attempted to identify the optimal conditions for using this approach.

Experimental

$La_xSr_{1-x}FeO_3$ (LSF) powders with various La:Sr ratios were synthesized via a standard sol-gel method.[4,8] The appropriate amounts of $La(NO_3)_3 \cdot 6H_2O$ (Alfa Aesar, 99%), $Sr(NO_3)_2 \cdot 4H_2O$ (Alfa Aesar, 99.0%), and $Fe(NO_3)_3 \cdot 9H_2O$ (Alfa Aesar, 98.5%) were dissolved in distilled water with citric acid (Fisher Scientific, 1:1 ratio with the metal cations) as the complexing agent. These solutions were dried at 373 K until a gel formed, after which they were calcined in air at 1473 K to form the perovskite. XRD analysis of the resulting powders showed only peaks characteristic of the perovskite phase. Throughout the remainder of this paper we will use the nomenclature LSFnm, where n:m corresponds to the La:Sr ratio, to specify the composition of each LSF sample. For example, LSF91 has a La:Sr ratio of 9:1. The YSZ powder was purchased from Tosoh (TZ-8Y) and contained 8% Y_2O_3.

Mixtures of the LSF and YSZ powders were prepared using a roller ball mill. The desired amounts of each powder were placed into an HDPE bottle together with zirconia beads. Ethanol was added as a solvent and the powders were milled for 12 h. The ethanol was then removed and the powders milled for an additional 12 h. After drying, the mixed LSF-YSZ powders were used without further processing. Since the LSF-YSZ mixtures were to be co-fired with the green YSZ electrolyte during cell fabrication, we calcined samples of the LSF-YSZ mixtures to 1623 K for 4 h. After calcination, the samples were ground into fine powders and analyzed using XRD to determine the extent of solid-state reactions.

The total conductivities of dense, pure-LSF and LSF-YSZ composite slabs were measured using the 4-probe method on slabs having dimensions of 7 mm × 3 mm × 1 mm. The slabs were prepared by pressing the LSF or mixed LSF-YSZ powders, followed by firing to 1623 K. The ionic conductivities of LSF82 and a 40-wt% LSF82/60-wt% YSZ composite were measured using a membrane reactor described in more detail in other publications.[8–10] Briefly, dense pellets of the mixed-conducting oxides, 330-μm thick and 1-cm diameter, were prepared by sintering the pressed powders to 1623 K for 4 h. To minimize resistance to surface reactions, porous layers of LSF82, ~30 μm thick, were fastened onto both sides of the LSF82 pellet using xylene; and similar porous layers of LSF82-YSZ were fastened onto the composite pellet. For both pellets, the porous layer on one side was impregnated with two rounds of the nitrate salts of La, Sr, and Fe to enhance oxygen adsorption, while the porous layer on the other side was infiltrated with 1-wt% Pd and 5-wt% ceria using their nitrate solutions (tetraammineplatinum(II) nitrate, Alfa Aesar; and $Ce(NO_3)_3 \bullet 6H_2O$, Alfa Aesar, 99.5%) to enhance reactions with CO.

*Electrochemical Society Member.
[z]E-mail: vohs@seas.upenn.edu

The pellets were then mounted onto a YSZ tube with a commercial sealant (ElectroScience 4461), cured in ambient air at 1123 K, cooled to room temperature, and inspected for cracks. After heating the samples, the Pd-containing side was exposed to flowing CO (12 ml/min) and the other side exposed to air. Oxygen-ion fluxes were determined from the rate of CO oxidation, measured using a gas chromatograph (Buck Scientific 910) with a Carboxen 1000 column (Supelco) and a thermal conductivity detector. Finally, the ionic conductivities were calculated from the oxygen flux and the chemical potential across the membrane, as described elsewhere.[10]

The electrochemical cells in this study were fabricated by tape-casting methods. We first laminated green tapes that contained graphite pore formers onto both sides of a YSZ tape without pore formers, followed by firing in air to 1623 K, to produce a porous-dense-porous structure. The YSZ electrolytes in these wafers were 80-μm thick and 1-cm in diameter, while the porous scaffolds were 35-μm thick, 0.70-cm in diameter, and 55% porous. Cells were made with scaffolds that were either pure YSZ, a 50-wt% LSF91-YSZ composite, or pure LSF91. The porous electrode tapes were manufactured using a Mistler tape caster and slurries containing the oxide powders mixed with ethanol (Decon, 100%), xylene, (Sigma-Aldrich, 98.5%), a dispersant (Blown Menhaden Fish Oil, Tape Casting Warehouse), a binder (Polyvinyl Butyl B-79, Tape Casting Warehouse), plasticizers (benzyl butyl phthalate, Sigma-Aldrich, 98%), and polyethylene glycol (Alfa Aesar). Pore formers (graphite, Sigma-Aldrich) were also added to the scaffold tapes. Additional details on the tape-casting procedures can be found in previous publications.[11,12] In some cases, the porous layers were infiltrated with $La_{0.6}Sr_{0.4}Co_{0.2}Fe_{0.8}O_{3-\delta}$ using an aqueous solution of $La(NO_3)_3 \cdot 6H_2O$ (Alfa Aesar, 99%), $Sr(NO_3)_2 \cdot 4H_2O$ (Alfa Aesar, 99.0%), and $Fe(NO_3)_3 \cdot 9H_2O$ (Alfa Aesar, 98.5%), each in their stoichiometric amounts. The final concentration of the solution was 1.3 M in $La(NO_3)_3$. Each infiltration cycle consisted of filling the pores with the precursor solution, followed by drying and calcination in air at 723 K to decompose the nitrates. After the final infiltration step, the cell was calcined in air at 1123 K to form the LSCF perovskite phase. For the porous scaffolds in this study, the final weight gains of LSCF after two and eight rounds were approximately 10% and 30%, respectively.

For cell testing, Ag paste (Lot No. 1191013, SPI Supplies) was applied to the electrodes for current collection. Impedance spectra were collected in air at 973 K and 1073 K using a Gamry Instruments impedance spectrometer.

Results and Discussion

A major goal in this work was to increase the electronic conductivity of the LSF-YSZ scaffold so that infiltration of LSCF would be required for catalytic purposes only. Because the conductivity of LSF increases with the level of Sr doping, we first examined the effect of Sr content on LSF-YSZ mixtures. Figure 1 shows a series of XRD patterns for mixtures of LSF and YSZ, after calcination to 1623 K. Figure 1a provides a wider view of the pattern, demonstrating that there are no extra phases, while a narrower view showing peak-position shifts is shown in Figure 1b. Both the weight percent LSF and the La:Sr ratio were varied. In separate experiments with graphite for a reference, the peaks associated with YSZ showed negligible shifts, in agreement with other reports.[5,7] The bottom pattern was obtained on a 50-wt% mixture of LSF82 and YSZ, prior to calcination, and shows features at 30.11 and 32.26 2θ corresponding to the (111) and (020) peaks of YSZ and LSF82, respectively. XRD patterns for physical mixtures of YSZ and LSF64 and LSF91 were essentially indistinguishable prior to calcination. Although the position of the (020) peak should change with La:Sr ratio, the shifts are small compared to the linewidth of the peaks shown here. None of the LSF-YSZ samples calcined at 1623 K showed evidence for new phases, but the peak positions for the perovskite phase shifted to lower angles in all cases. This result is consistent with previous reports for co-fired LSF-YSZ mixtures.[5,7] The shift in the perovskite lattice parameter is believed to be caused by Zr cations dissolving into the perovskite lattice.

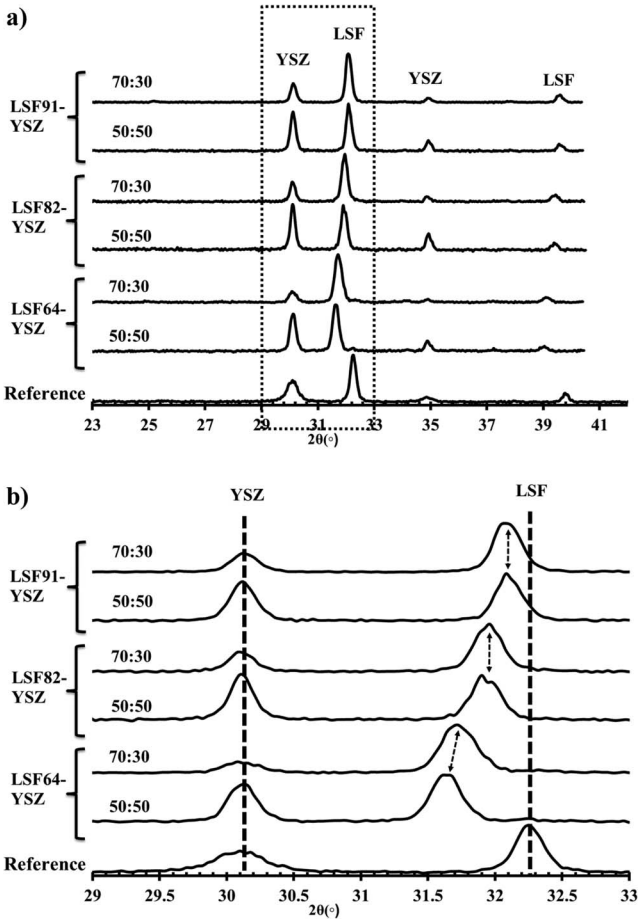

Figure 1. XRD patterns of LSF-YSZ mixtures after calcination at 1623 K for 4 h with different LSF:YSZ weight ratios (as indicated in the figure) and different La:Sr ratios in the LSF. The bottom pattern is that of a physical mixture of a 50-wt% LSF91-YSZ mixture prior to calcination. (a) shows the XRD patterns over a wider range of angles while (b) reports the same patterns in the region shown between the dashed lines in (a).

A closer look at the XRD patterns shows that the peak shift for the perovskite phase increases with Sr content. Considering only the 50-wt% LSF-YSZ samples, the (020) perovskite peak decreased to 32.12 degrees 2θ for the LSF91-YSZ sample, 31.96 degrees 2θ for the LSF82-YSZ sample, and 31.68 degrees 2θ for the LSF64-YSZ sample. The larger peak shift would suggest an increased level of Zr doping. When we increased the weight percent of perovskite in the LSF-YSZ mixtures to 70-wt% LSF, the position of the perovskite diffraction peak on the LSF91-YSZ and LSF82-YSZ samples did not change, suggesting that the two phases were essentially in equilibrium, with Zr doping having reached its saturation limit. For the 70-wt% LSF64-YSZ sample, the YSZ peak almost disappeared and the shift in the perovskite peak was significantly lower, implying that the YSZ phase had been almost completely consumed into the perovskite phase. This is again consistent with increased Zr doping for materials with higher Sr:La ratios.

Ultimately, the goal in preparing LSF-YSZ composites is to increase the conductivity of the scaffold. The results from 4-probe conductivity measurements at 973 K of dense LSF and 50-wt% LSF-YSZ composites are shown in Figure 2 as a function of the La:Sr ratio. The previously reported value for the conductivity of LSF82 agrees well with our present measurements.[7] The conductivity of pure LSF decreases monotonically as the Sr content decreases, from approximately 160 S/cm for LSF64 to 25 S/cm for $La_{0.95}Sr_{0.05}FeO_3$. However, the conductivities of the 50-wt% LSF-YSZ mixtures go through a maximum near the La:Sr ratio of 9. Furthermore, the conductivities of the composites are a small fraction of the pure LSF conductivities. Based

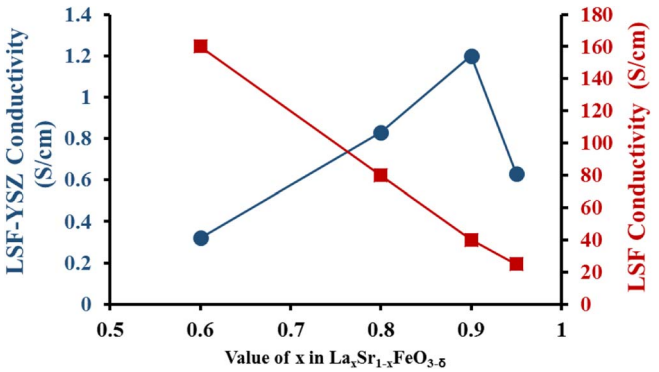

Figure 2. Total conductivity of dense 50-wt% LSF:YSZ composites and pure LSF as a function of the La:Sr ratio in the LSF.

on previous work with composites of Sr-doped $LaCrO_3$ (LSCr) and YSZ,[8] a 40-wt%, random composite of a conductor and an insulator would have a conductivity approximately 5% of the pure electronic conductor. In the present study, a 50-wt% LSF64-YSZ composite exhibited a conductivity only 0.2% that of LSF64 and a 50-wt% LSF91-YSZ composite exhibited a conductivity that was 3% that of LSF91. These results imply that the Zr doping decreases the electronic conductivity of the perovskite and that the loss in conductivity decreases with Sr content.

The scaffold ionic conductivity is another factor that influences electrode performance.[12,13] Both experiments and theory have shown that electrode impedances should vary with the inverse square root of this parameter if all other factors remain constant.[13] In the present study, we measured the ionic conductivity of dense LSF82 and 40-wt% LSF82-YSZ composites using a membrane reactor to determine the effect of Zr dissolution into the LSF phase. Figure 3 shows the measured oxygen fluxes through LSF82-YSZ and LSF82 membranes as a function of temperature, with CO flowing on one side of the membrane and the other side exposed to air. The oxygen fluxes were calculated from the CO conversion to CO_2, measured using a gas chromatograph. As discussed elsewhere,[9,10] the total resistance of the mixed-conducting membrane to oxygen flow can be calculated from these measurements. By applying catalytic electrodes to the surfaces of the membrane, the surface resistances become small, making ion conduction the limiting factor.

The new data for the ionic conductivities of LSF82 and LSF82-YSZ at 973 and 1073 K are summarized in Table I together with previously reported data for the ionic conductivities of $La_{0.9}Ca_{0.1}FeO_3$[9] and the tabulated conductivity of YSZ.[14] It is interesting to notice that, at 973 K, the ionic conductivity of LSF82, 0.072 S/cm, is about twice that of $La_{0.9}Ca_{0.1}FeO_3$, 0.03 S/cm. The major difference here is likely the higher dopant level in LSF82. Although it has been suggested that Sr-doped materials could have higher ionic conductivities than their Ca-doped analogs,[15–17] this does not appear to be the case.

More significant for our purposes here, the ionic conductivity of the 40-wt% LSF82-YSZ composite at 973 K was only 0.006 S/cm,

Table I. Ionic conductivities of dense materials used in this study. Results for the 40-wt% LSF82-YSZ composite and LSF82 were determined from oxygen fluxes measured in a membrane reactor. Data for LCF and YSZ were taken from References 9 and 14.

Temperature (K)	40-wt% LSF82-YSZ (S/cm)	LSF82 (S/cm)	LCF91 (S/cm)	YSZ8 (S/cm)
973	0.006	0.072	0.03	0.019
1073	0.017	0.089	0.07	0.042

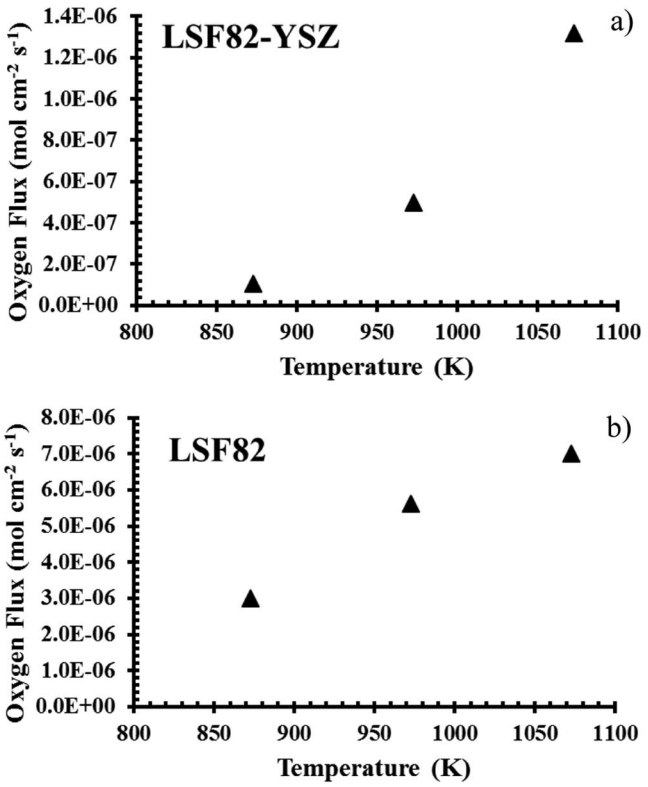

Figure 3. Oxygen fluxes as a function of temperature measured in a membrane reactor using flowing CO on one side and air on the other. Data are shown for a) a dense, 40-wt% LSF82-YSZ membrane and b) an LSF82 membrane. Both membranes were 330 μm thick, with catalyst layers on both sides to reduce surface resistances.

a value that is much less than that of either YSZ (0.019 S/cm) or LSF82. Interestingly, the ionic conductivity of a 40-wt% LSCr-YSZ composite at 973 K was shown to be almost the same value, 0.0046 S/cm.[8] Since the ionic conductivity of LSCr is likely negligible, most of the ionic conductivity in the LSCr-YSZ membranes was due to the YSZ. With LSF82-YSZ, the perovskite phase may be contributing but the low value suggests that Zr doping has significantly reduced the ionic conductivity of the perovskite phase.

To determine the effect of scaffold properties on electrode performance, we compared symmetric cells made with pure YSZ scaffolds, with 50-wt% LSF91-YSZ composite scaffolds, and with pure LSF91 scaffolds. The scaffold made with pure LSF91 should have the highest electronic conductivity but could have a low ionic conductivity in the electrochemically active region since Zr doping near the electrolyte interface will be important. The pure YSZ scaffold likely has the highest ionic conductivity but negligible electronic conductivity, while the composite scaffold will be a compromise, at least with respect to electronic and ionic conductivities.

Figures 4a and 4b show impedance data at 973 K and 1073 K in air for symmetric cells made from each of the scaffolds. Data were taken with zero, two, and eight infiltration cycles of LSCF. In the absence of infiltrated LSCF, all three cells exhibited ohmic resistances in excess of that expected for the YSZ electrolyte. (Because the Nyquist Plots have been divided by two to account for the two electrodes, the contribution from the 80-μm electrolyte is expected to be 0.2 $\Omega \cdot cm^2$ at 973 K and 0.1 $\Omega \cdot cm^2$ at 1073 K.) For pure YSZ at 973 K, the excess ohmic losses were nearly 2.5 $\Omega \cdot cm^2$ greater than the electrolyte resistance prior to infiltration. For the LSF91 and LSF91-YSZ scaffolds in the absence of infiltration, the ohmic resistances at 973 K were only 0.14 and 0.3 $\Omega \cdot cm^2$ in excess of the expected 0.2 $\Omega \cdot cm^2$.[2] In the present study, the scaffolds were 35-μm thick and some of extra ohmic resistance could be reduced by using thinner scaffold layer. Since a typical electrode

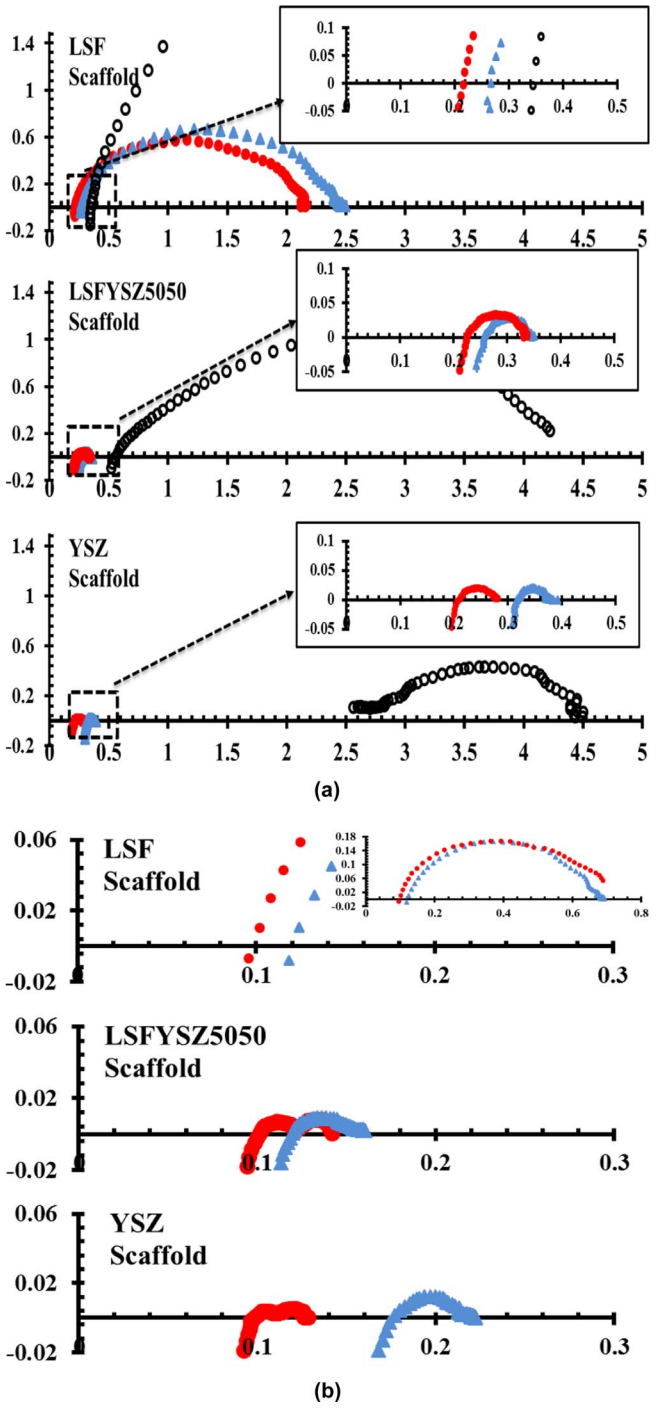

Figure 4. Nyquist plots of symmetric cells with different cathode scaffolds in air as a function of the number of infiltration rounds in the scaffold. Hollow symbols (**O**) are for cells with bare scaffolds and filled symbols are for cells with two rounds (▲) and eight rounds (●) of infiltration of LSCF. Data are shown at 973 K in (a) and 1073 K in (b).

functional layer is less than one-third this value, thinner scaffolds could certainly be employed.[18]

With the pure YSZ scaffold, two infiltration cycles of LSCF reduced the excess ohmic to 0.1 $\Omega \cdot cm^2$ above the expected electrolyte resistance at 973 K and 0.07 $\Omega \cdot cm^2$ at 1073 K. Eight infiltration cycles resulted in cells with the correct ohmic resistance. The non-ohmic losses in cells with eight infiltration cycles were less than 0.1 $\Omega \cdot cm^2$ at 973 K and 0.03 $\Omega \cdot cm^2$ at 1073 K. Similarly, infiltration of eight cycles of LSCF decreased the ohmic losses in cells with LSF91-YSZ and LSF91 scaffolds to the resistance of the electrolyte. The non-ohmic resistance of the fully infiltrated LSF91-YSZ scaffolds was slightly larger than that of infiltrated YSZ scaffolds, possibly due to LSF91-YSZ scaffolds having a smaller ionic conductivity than pure YSZ scaffolds. As previously stated, the non-ohmic resistance is negatively correlated with the ionic conductivity of the scaffold. However, while the non-ohmic losses in cells with the LSF91-YSZ scaffold was close to that achieved with the YSZ scaffold after two infiltration cycles, the non-ohmic losses with the LSF91 scaffold remained very large, ~2 $\Omega \cdot cm^2$ at 973 K.

In order to understand the possible reasons for the poor performance of cells prepared with LSF91 scaffolds, cross-sectional SEM images were taken of the electrolyte-scaffold interface on cells similar to those used in Figure 4. The images shown in Figure 5 demonstrate the likely reason for the poor performance of the cell with the pure LSF electrode scaffold. (These images are of the scaffold without infiltrated nanoparticles; images of the nanoparticles are reported elsewhere.[5]) The image in Figure 5a is that of a cell with a pure YSZ scaffold. The electrode scaffold produced using graphite pore formers has uniformly distributed pores with diameters of ~2 μm, and the interface between the scaffold and the electrolyte shows good connectivity. The image in Figure 5b is that of a cell with a 50-wt% LSF91-YSZ scaffold. The scaffold structure again shows uniform pores but ones that are slightly larger, 5 to 10 μm in diameter. The reason for the larger pores is uncertain but likely related to the different sintering properties of LSF and YSZ. The scaffold-electrolyte interface again shows good bonding. These results are in contrast to what we observed for the cell with the pure LSF91 scaffold. As shown in Figure 5c, this scaffold contained pores that were greater than 20 μm in diameter and the scaffold was poorly connected to the YSZ electrolyte. The poor connectivity with the electrolyte is an especially serious problem.

While it may be possible to engineer a better electrolyte-scaffold interface in cells with LSF scaffolds, there are fundamental issues that make this difficult. In order to form a good interface in laminated layers, the two layers need to shrink simultaneously during calcination. However, shrinkage and densification in pressed LSF pellets typically occurs at much lower temperatures, as low as 1273 K,[19] while temperatures in excess of 1623 K are typically needed to sinter YSZ.[20] Therefore, the poor microstructure at the YSZ-LSF91 interface is likely due to this difference in the sintering rates for the LSF91 and YSZ. This conclusion is also supported by the SEM images which show that the pure LSF91 scaffold (Figure 5c) appears to have much larger grain sizes compared to what is observed in YSZ and YSZ-LSF91 composite scaffold. If the LSF particles could be modified to sinter at a similar temperature as YSZ, it may be possible to improve the interface contact.

While there is still much work required in order to understand the long-term stability of SOFC cathodes prepared by infiltration, the present study demonstrates that it should be possible to co-fire an electronically conductive scaffold based on LSF and YSZ together with a YSZ electrode, reducing the required number of calcination steps in cell fabrication. The use of these electronically conductive scaffolds decreases the number of infiltration steps required to prepare high-performance electrodes. Preparation of cathodes by infiltration into co-fired scaffolds should also eliminate the need for adding a barrier layer between the cathode and the electrolyte, which can also add to the cell resistance.[21] Therefore, infiltration into conducting scaffolds has the potential to be very attractive for improving SOFC performance and reducing the cost of cell fabrication.

Summary

High-performance SOFC cathodes can be prepared by infiltration of LSCF into porous scaffolds that have been co-fired together with YSZ electrolytes. By using scaffolds made from electronically conductive, LSF-YSZ mixtures, the number of LSCF infiltration steps can be greatly reduced. LSF and YSZ can be co-fired to 1623 K without forming new insulating phases; however, Zr doping of the perovskite phase does decrease both its electronic and ionic conductivity. Zr

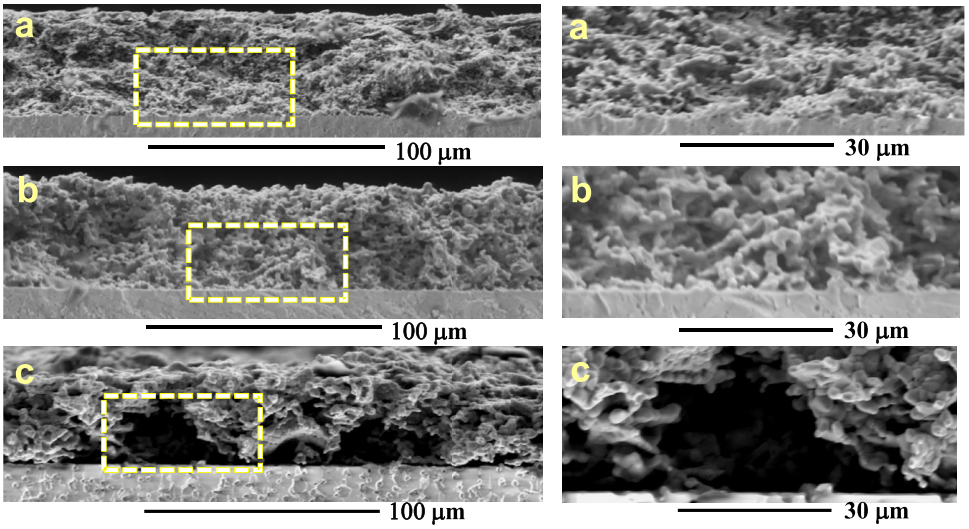

Figure 5. Scanning Electron Micrographs of co-fired scaffold-YSZ electrolyte interfaces. Data are show for (a) a pure YSZ scaffold, (b) a 50:50 LSF91-YSZ composite scaffold and (c) a pure LSF91 scaffold.

doping in the perovskite phase of LSF-YSZ mixtures calcined to 1623 K also increases with the Sr:La ratio. Since the conductivity of pure LSF also increases with Sr:La ratio, there is an optimum Sr:La ratio near $La_{0.9}Sr_{0.1}FeO_3$ for the LSF used in LSF-YSZ composites.

Acknowledgments

This material is based upon work supported by the Department of Energy under Award Number DE-FE0023317. This report was prepared as an account of work sponsored by an agency of the United States Government. Neither the United States Government nor any agency thereof, nor any of their employees, makes any warranty, express or implied, or assumes any legal liability or responsibility for the accuracy, completeness, or usefulness of any information, apparatus, product, or process disclosed, or represents that its use would not infringe privately owned rights. Reference herein to any specific commercial product, process, or service by trade name, trademark, manufacturer, or otherwise does not necessarily constitute or imply its endorsement, recommendation, or favoring by the United States Government or any agency thereof. The views and opinions of authors expressed herein do not necessarily state or reflect those of the United States Government or any agency thereof.

References

1. L. Blum, L. G. J. (Bert) de Haart, J. Malzbender, N. H. Menzler, J. Remmel, and R. Steinberger-Wilckens, *J. Power Sources*, **241**, 477 (2013).
2. J. M. Vohs and R. J. Gorte, *Adv. Mater.*, **21**, 943 (2009).
3. R. Küngas, F. Bidrawn, J. M. Vohs, and R. J. Gorte, *Electrochem. Solid-State Lett.*, **13**, B87 (2010).
4. Y. Cheng, A. S. Yu, X. Li, T.-S. Oh, J. M. Vohs, and R. J. Gorte, *J. Electrochem. Soc.*, **163**, F54 (2016).
5. W. Wang, M. D. Gross, J. M. Vohs, and R. J. Gorte, *J. Electrochem. Soc.*, **154**, B439 (2007).
6. M. D. Anderson, J. W. Stevenson, and S. P. Simner, *J. Power Sources*, **129**, 188 (2004).
7. S. P. Simner, J. P. Shelton, M. D. Anderson, and J. W. Stevenson, *Solid State Ionics*, **161**, 11 (2003).
8. A. S. Yu, T.-S. Oh, R. Zhu, A. Gallegos, R. J. Gorte, and J. M. Vohs, *Faraday Discuss.*, **182**, 213 (2015).
9. A. S. Yu, J. Kim, T. S. Oh, G. Kim, R. J. Gorte, and J. M. Vohs, *Appl. Catal. A Gen.*, **486**, 259 (2014).
10. A. S. Yu, J. M. Vohs, and R. J. Gorte, *Energy Environ. Sci.*, **7**, 944 (2014).
11. M. Boaro, J. M. Vohs, and R. J. Gorte, *J. Am. Ceram. Soc.*, **86**, 395 (2003).
12. R. Küngas, J. M. Vohs, and R. J. Gorte, *J. Electrochem. Soc.*, **158**, B743 (2011).
13. F. Bidrawn, R. Küngas, J. M. Vohs, and R. J. Gorte, *J. Electrochem. Soc.*, **158**, B514 (2011).
14. V. V. Kharton, F. M. B. Marques, and A. Atkinson, *Solid State Ionics*, **174**, 135 (2004).
15. F. Bidrawn, S. Lee, J. M. Vohs, and R. J. Gorte, *J. Electrochem. Soc.*, **155**, B660 (2008).
16. S. Li, W. Jin, P. Huang, N. Xu, J. Shi, M. Z. Hu, and E. A. Payzant, *Ind. Eng. Chem. Res.*, **38**, 2963 (1999).
17. J. W. Stevenson, T. R. Armstrong, R. D. Carneim, L. R. Pederson, and W. J. Weber, *J. Electrochem. Soc.*, **143**, 2722 (1996).
18. V. A. C. Haanappel, J. Mertens, and A. Mai, *J. Fuel Cell Sci. Technol.*, **3**, 263 (2006).
19. L. T. Sagdahl, M. A. Einarsrud, and T. Grande, *J. Eur. Ceram. Soc.*, **26**, 3665 (2006).
20. E. Courtin, P. Boy, T. Piquero, J. Vulliet, N. Poirot, and C. Laberty-Robert, *J. Power Sources*, **206**, 77 (2012).
21. A. Martinez-Amesti, A. Larranaga, L. M. Rodriguez-Martinez, M. L. No, J. L. Pizarro, A. Laresgoiti, and M. I. Arriortua, *J. Electrochem. Soc.*, **156**, B856 (2009).